This document is a manuscript of:
Szczypiński, P. M.
Radius Estimation in Angiograms Using Multiscale Vesselness Function.
In International Conference on Computational Science (pp. 230-244).
(2023, June). Cham: Springer Nature Switzerland.
https : *//doi.org*/10.1007/978 − 3 − 031 − 36027 − 5_17

Radius Estimation in Angiograms using Multiscale Vesselness Function

Piotr M. Szczypiński[1][0000−0002−9956−0862]

Institute of Electronics, Lodz University of Technology, Lodz, Poland
piotr.szczypinski@p.lodz.pl

Abstract. This paper presents a new method for estimating the radius of blood vessels using vesselness functions computed at multiple scales. The multiscale vesselness technique is commonly used to enhance blood vessels and reduce noise in angiographic images. The corrected and binarized image resulting from this technique is then used to construct a 3D vector model of the blood vessel tree. However, the accuracy of the model and consequently the accuracy of radii estimated from the model may be limited by the image voxel spacing. To improve the accuracy of the estimated vessel radii, the method proposed in this study makes use of the vesselness functions that are already availabe as by-products of the preceding enhancement procedure. This approach speeds up the estimation process and maintains sub-voxel accuracy. The proposed method was validated and compared with two other state-of-the-art methods. The quantitative comparison involved artificially generated images of tubes with known geometries, while the qualitative assessment involved analyzing a real magnetic resonance angiogram. The results obtained demonstrate the high accuracy and usefulness of the proposed method. The presented algorithm was implemented, and the source code was made freely available to support further research.

Keywords: Radius estimation · Vesselness · Angigram analysis

1 Introduction

One of the key challenges in angiographic image analysis is to accurately estimate the radius of veins and arteries [3,6]. These estimated radii form an input data for three-dimensional modeling of vessel structures [6,37,27,4,30,11] which are used for data visualization, surgical planning, and medical diagnosis support [30,18,17,29,13]. Analyzing the radii along the blood vessels facilitates the detection of lesions such as stenosis and aneurysm.

Angiograms, MRA or CT scans, are raster images of voxels arranged in three-dimensional arrays, which are difficult to quantify directly for medical diagnosis. They need to be converted into a more convenient vector representation. One common way to represent image objects in vector form is by surfaces of triangular meshes that define approximate boundaries between anatomical structures [26,8,7]. Alternatively, elongated, tubular structures can be described by their

centerlines and radii functions defined along these centerlines [37,40,20]. Both approaches can be used as vector models for the blood vessel system. As blood flows under certain pressure, the vessel walls are inflated and adopt a circular cross-sectional shape. Therefore, the second representation with centerlines and radii is reasonable, and what's more, it directly facilitates quantitative morphological attributes for stenosis or aneurysm detection.

Converting the angiographic raster data to a vector representation involves several processing steps. The first step is filtering the raster image with multiscale vesselness, which enhances blood vessels and reduces image noise [15,10,5,33]. Next, the image is binarized [23,32,35,43] to assign each voxel a label indicating its location inside or outside the blood vessel. Image binarization can be performed using algorithms such as active contours [42,44] , level-set methods [8,39] , or deep learning neural networks [25,12,31,24,34], There are two alternative methods for producing centerlines from the binary image. The first approach is to apply marching cubes or a similar algorithm to find the polygonal mesh of the vessel's surface, which is then smoothed and collapsed to form the centerline [29,23,14]. The other method is skeletonization [13,22,41] of the binary image, which thins the structures of blood vessels consisting of white voxels to form a single-voxel-thick line. The resulting centerline may appear rough and requires smoothing in the next step through low-pass filtering of voxel chain coordinates.

This paper presents an original algorithm for radius estimation from multiscale vesselness (REMV), assuming that centerlines and sub-results of multiscale vesselness computation are available. The proposed method is validated and compared with two state-of-the-art methods, one extracting information from the binary image and the other estimating the radius from the original gray-scale image with presumably sub-voxel accuracy. The experiments use artificially generated images of tubes with known geometries for quantitative comparison and a real magnetic resonance angiogram for practical yet qualitative assessment of the results.

2 Methods

2.1 Vesselness-radius relationship

The vesselness function algorithm [15,10,5,33,21,1] is used to identify tubular structures in a raster image, and it is particularly useful in the analysis of angiograms. This algorithm enhances the contrast between blood vessels and surrounding tissues, reduces image noise, and conceals anatomical structures that are not cylindrical in shape.

The computation of the vesselness function involves several steps. First, the image is blurred using the Gaussian kernel function with a standard deviation σ. The value of σ should be adjusted according to the radius of the vessel. Second, the Hessian matrices, which are square matrices of second-order partial derivatives of the image intensity function, are computed at every voxel of the image. The matrices are eigen-decomposed, and it has been observed [10] that

the relations between eigenvalues determine the shape of the structures that are locally present in the image. In tubular structures, one of the eigenvalues is close to zero, while the absolute values of the other two eigenvalues are significantly greater and their values are close to each other.

Several formulas have been proposed to compute the vesselness function from these eigenvalues, including those developed by Erdt [5] , Frangi [10,9] and Sato [33]. In this context, we will discuss the formula developed by Sato. In his approach, the eigenvalues are ordered from the largest to the smallest $\lambda_1 \geq \lambda_2 \geq \lambda_3$. The vesselness formula proposed by Sato has a form similar to equation (1). However, the equation presented below includes an additional factor σ^2.

$$F = \sigma^2 \begin{cases} \lambda_c \exp\left(-\frac{\lambda_1^2}{2(\alpha_1 \lambda_c)^2}\right) & : \ \lambda_1 \leq 0, \ \lambda_c \neq 0 \\ \lambda_c \exp\left(-\frac{\lambda_1^2}{2(\alpha_2 \lambda_c)^2}\right) & : \ \lambda_1 > 0, \ \lambda_c \neq 0 \\ 0 & : \ \lambda_c = 0 \end{cases} \tag{1}$$

$$\lambda_c = \min(-\lambda_2, -\lambda_2) \quad \alpha_1 = 0.5 \quad \alpha_2 = 2$$

Setting a proper value of the standard deviation σ is essential for correct enhancement of structures having a particular radius. This parameter should be set according to the actual radius of the blood vessels being enhanced. Fig. 1 illustrates this principle using cross-section of an example cylinder for which the vesselness was computed for various values of σ. If this parameter is significantly smaller than the radius of the cylinder, only the elements near the walls are exposed. If it is much larger than the radius, the vesselness appears blurry. The vessel is bright and properly exposed if the σ value is close to the actual radius of the cylinder. Because different values of σ allow for proper enhancement of structures with different radii, σ is sometimes referred to as the scale of the vesselness function. The dependence of the vesselness function on the value of σ is essential for the proposed in here radius estimation algorithm.

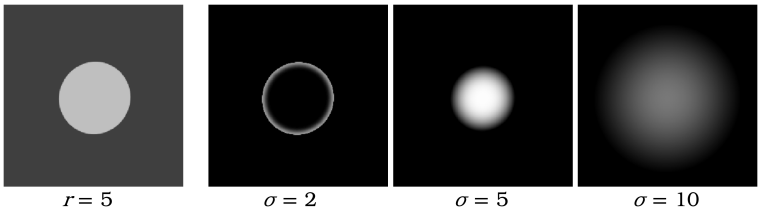

Fig. 1. A cross-section of a cylindrical structure and its vesselness function for various standard deviations of the Gaussian blurring.

If an angiogram consists of a number of vessels having different radii, several vesselness functions can be computed for varying values of the σ parameter. The range of σ variability should cover the range of radii variability. The result-

ing images obtained for different values of σ are then combined in a so-called multiscale vesselness function.

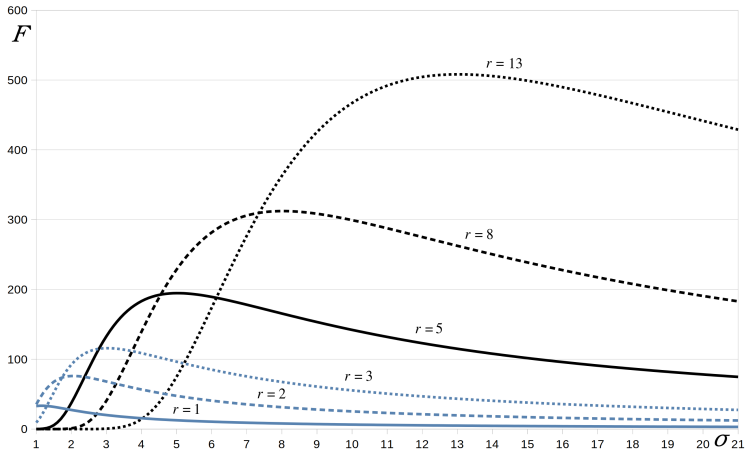

Fig. 2. The vesselness computed at centers of cylinders of various radii as a function of the standard deviation.

An experiment was carried out to compute the vesselness along cylinders of various radii ($r = 1, 2, 3, 5, 8, 13$). Ten cylinder images with random orientation were synthesized for each radius. The vesselness functions were computed for the images using standard deviations σ ranging from 1 to 21. The resulting plots of vesselness obtained at the centers of the cylinders are shown in Fig. 2. It was observed that the plots reached their maxima at the σ argument equal to the radius of the cylinder. This property leads to the conclusion that the radius of a blood vessel can be estimated from such a plot by finding the maximum. Thus, the proposed algorithm consists of computing the vesselness function (1) as a function of the standard deviation of the Gaussian blurring filter. The argument σ at the maximum of the function becomes an estimate of the radius.

2.2 Curve fitting to estimate vessel radius

To indicate the maximum of the vesselness function with sufficiently high accuracy, the function should be computed for densely distributed values of the σ parameter. Such the approach requires numerous computations of the vesselness functions which is computationally demanding and thus time consuming. What is more, the multiscale vesselness function intended for image enhancement is usually computed for a limited number of scales. To keep the method computationally efficient and accurate, a limited number of vesselness measurements can be approximated with a curve. The σ argument at the maximum of the curve would then estimate the radius of the vessel.

Vesselness computation is a complex procedure, and furthermore, raster images cannot be defined in an analytic form. Therefore, it is infeasible to derive an equation or mathematical model that would accurately define such the curve. Instead, in order to find a suitable equation to define the curve, a number of unimodal function formulas were reviewed. As a result, a formula (2) inspired by the transfer functions of analog filters was selected, which most closely matched all the plots. The equation consists of two factors. The first one, with parameters A and κ, is responsible for modeling the falling slope of the curve for $\sigma > r$. The second factor, with parameter η, models the rising slope of the curve for $\sigma < r$.

$$f(\sigma; A, r) \;=\; \frac{A\omega r\kappa}{\sqrt{1+\kappa^2\left(\frac{\sigma}{\omega r}-\frac{\omega r}{\sigma}\right)^2}}\left(\frac{\left(\frac{\sigma}{\omega r}\right)^2}{1+\left(\frac{\sigma}{\omega r}\right)^2}\right)^{\eta} \tag{2}$$

The values of parameters κ, ω and η were optimized to adjust the formula to fit the family of functions in Fig. 2. As a result, the three constants were established: $\kappa = 17.289$, $\omega = 0.03411$ and $\eta = 432$. The other two parameters, A and r, allow for adjusting the mathematical model to specific data. The A parameter scales the function's value, while r scales it in the argument domain. Such the model facilitates a near-perfect mapping of the empirical data, with the mean square error not exceeding 0.28. It should be noted that the function (2) obtains the maximum when σ equals r. Therefore, after fitting the formula, the parameter r becomes an estimator of the radius.

2.3 Reference methods

Our goal is to compute the radii of vessels along their centerlines. Typically, radii are estimated for a number of evenly spaced points along the centerline. For each of these points, the local direction of the centerline can be estimated, taking into account the location of neighboring points. Therefore, it is possible to determine the plane perpendicular to this direction, which contains the considered point. This reduces the problem of radius computation in the three-dimensional image space to the two-dimensional space of the vessel's cross-section [3,13,23,38].

In the 2D cross-sectional image, radius estimation consists of determining the distance between the centerline point and the vessel wall. A number of such distances are sampled around the point along concentrically distributed directions, or rays, which are evenly distributed with equal angular intervals. The local radius may be computed by averaging the distances. Typically, the radius is computed as the square root of the averaged squares of the distances. Thus, the resulting radius corresponds to a circle with an area equal to the area of the actual cross-section of the vessel.

Finding the location of the vessel wall along the ray can be accomplished in several ways. One approach involves using a binary image as input, with white voxels representing the inside of the blood vessel and black voxels representing the surrounding tissue. Assuming that the voxels have the shape of small cuboids, the border between the black and white voxels approximates the shape of the wall

with accuracy determined by the image raster. The distance sample is defined as the distance between the centerline's point and the point of ray intersection with the nearest boundary between white and black voxels.

The algorithm for locating vessel wall samples in a binary image is computationally efficient and robust. It should be noted that the algorithm operates on binary images, which are visually verified and corrected by human expert to ensure that they accurately reflect the real anatomical structure. While this method accurately reflects the real topology of the blood vessel system, its accuracy is still limited by the resolution of the image. To achieve greater accuracy, information about the brightness distribution in the original image should be utilized. By incorporating this information into the search procedure, it is possible to locate anatomical structures with sub-voxel accuracy.

To find the position of the vessel wall with higher accuracy, a brightness profile along the ray is considered. The profile should be determined to a distance two times longer than the expected radius. This way, the profile equally represents the brightness of the inner and outer regions of the vessel. The profile is characterized by higher brightnesses in areas belonging to the inside of the vessel and significantly lower brightnesses representing the surrounding tissue. Therefore, a distinct slope in the brightness function, where the brightness suddenly drops, should indicate the localization of the vessel's wall.

The brightness profile is affected by various phenomena, including blurring caused by imperfections in the imaging devices. These phenomena can be modeled using the point spread function, which describes the response of the imaging system to a point source signal. Another factor that affects the brightness profile is the partial volume effect. Each voxel occupies a certain volume of three-dimensional space, and if it lies on the edge of two regions, it partially covers a piece of each region. As a result, its brightness is a weighted average of the brightness of both regions, taking into account the partial volumes of these regions covered by the voxel. One acceptable simplification is to model the point spread function of the device with a linear Gaussian blur filter. This allows the shape of the brightness profile near the border to be approximated with a complementary error function (erfc). The erfc function can be fitted to the brightness profile using formula (3), by adjusting the values of its four parameters (Δ_V, Δ_R, V_0 and r) to minimize the mean squared error between the model and the brightness profile [3,27]. After fitting the model to the brightness profile, the parameter r, which determines the shift in the function's domain, indicates the position of the blood vessel wall (Fig. 3).

$$u(d; \Delta_V, \Delta_R, V_0, r) \;=\; V_0 + \Delta_V \, erfc\left(\frac{(d-r)}{\Delta_R}\right) \tag{3}$$

In the following experiment, the proposed procedure, which applies the vesselness function for radius estimation, is compared with ray-casting methods. Two alternative approaches for vessel wall localization are used as reference methods: one to locate the wall in a binary image and the other to approximate the brightness profile with the complementary error function.

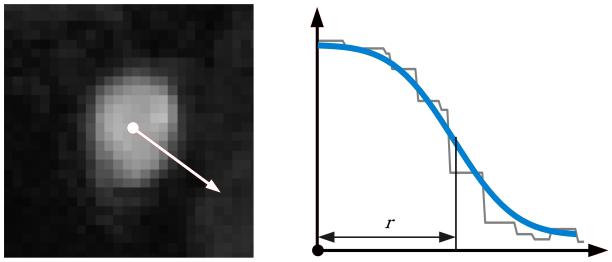

Fig. 3. Matching the complementary error function to the brightness profile.

3 Results

The three algorithms: radius estimation from multiscale vesselness (REMV), cross-sectional ray-casting in binary image (CRB) and cross-sectional ray-casting with erfc matching (CREM) were tested on artificially generated images of tubes and on real magnetic resonance angiogram (MRA). Artificial images of structures of known geometries enabled quantitative comparison and MRA image enabled qualitative, visual assessment. In ray-casting 360 directions were used. In CREM, the erfc was fitted to the brightness profiles consisting of 100 points each, linearly interpolated from the original image. In REMV, the vesselness function was calculated for geometric sequence of 7 scales of σ ranging from 0.5 to 15.

3.1 Radius estimation results in images of cylinders

In the first experiment, similarly to [3,27,19], synthetic images of cylinders (two examples are in Fig. 4) with dimensions $100\times100\times100$ voxels and 256 gray levels were generated. Each cylinder was positioned at the center of the image. Cylinders had varying radii of 1, 2, 3, 5, 8, and 13. For each radius value, 10 images were produced, each showing the cylinder in a different orientation. It was observed that for blood vessels located on the verge of two volumes with different brightness levels it is difficult to segment the image and accurately determine the radius of the vessel. Therefore, in every image, a sphere with a radius of 150, representing an internal organ, was located in such a way that its surface passed through the center of the image. The cylinders were set to a gray-level of 192, the sphere to 128, and the background to a dark gray value of 64. Partial volume effect was simulated. Finally, Gaussian noise with standard deviation values of 1, 2, 3, 5, 8, and 13 was added to the images. For the CRB procedure, the images were pre-binarized using a brightness threshold of 160, which is a value between the brightness of the sphere and the cylinder.

Fig. 4 shows the estimated radii profiles for selected cases of cylinders with real radii of 2 and 5. The radius estimations were computed at 80 points along the centerline. First 40 measurements correspond to the cylinder fragment outside the sphere, the other measurements are from the inside.

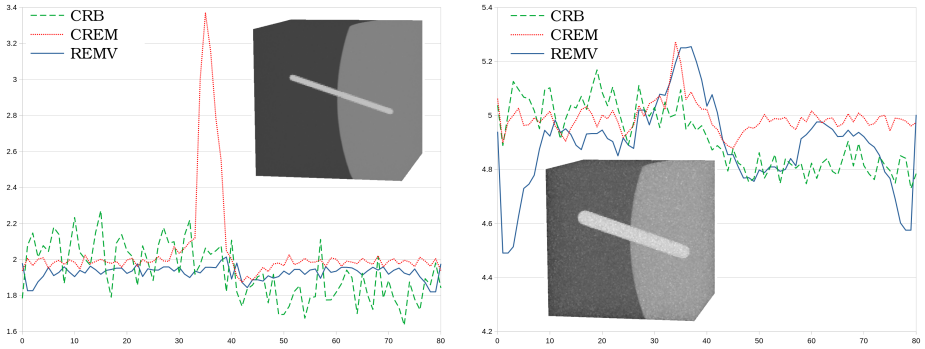

Fig. 4. Example cylinder images with radii of 2 and 5, and their estimated radii profiles.

CREM overestimates the radius in the dark region near the surface of the sphere, which is more pronounced in the thinner cylinder and less so in the thicker one. Both CREM and CRB underestimate the radius inside the bright sphere. The estimated radius plots in CRB are jittery, suggesting vulnerability to noise. In comparison, REMV seems insensitive to changes in the background gray level in the thinner cylinder, but in the thicker one, the radius is overestimated on one side and underestimated on the other side, similar to the results produced by the reference methods.

To make a quantitative comparison of the algorithms, the averages and standard deviations of radius estimates were computed for images with the same noise level and cylinders of the same radius. Table 1 presents these statistics for each algorithm with respect to the real radii and noise levels. The table also shows the total computation time for each algorithm.

Table 1. Average radius estimates and their standard deviations (in brackets) for the selected radii and noise levels.

Radius	Noise	CREM	CRB	REMV
1	1	1.52 (0.90)	0.92 (0.20)	1.02 (0.08)
1	5	1.51 (0.88)	0.93 (0.20)	1.03 (0.09)
1	13	1.44 (0.74)	0.94 (0.21)	1.06 (0.13)
5	1	5.01 (0.08)	4.91 (0.11)	4.85 (0.19)
5	5	5.01 (0.08)	4.91 (0.11)	4.86 (0.19)
5	13	5.01 (0.10)	4.90 (0.12)	4.86 (0.20)
13	1	12.94 (0.10)	12.91 (0.09)	12.63 (0.53)
13	5	12.44 (0.53)	12.91 (0.09)	12.64 (0.53)
13	13	8.21 (2.00)	12.90 (0.09)	12.64 (0.53)
	Time	02:06:41	00:00:39	00:18:36

In CREM, radii are overestimated for thin cylinders with radii similar to the size of the voxel, and the results show a relatively large standard deviation, indicating scattered results. Conversely, for thick cylinders and with the presence of noise, this method highly underestimates radii. CRB produces slightly underestimated values with moderate standard deviations, whereas REMV produces the most accurate estimates for thin cylinders and slightly underestimates radii for thicker ones. The computation time required for CREM was the highest, but it can be reduced by reducing the number of rays, which in this experiment was set high. CRB is the most efficient, and the computation time for REMV is moderate. However, the time for REMV includes the computation of multiscale vesselness, results of which can be shared by the REMV and image enhancement algorithms.

3.2 Radius estimation results in bifurcation image

In the next experiment, an image of a bifurcation (Fig. 5) was synthesized, which is a structure that often appears in a blood vessel system and is difficult to analyze, estimate radii, and model [3,15,19]. Bifurcations involve three branches of varying diameters, with one usually larger than the other two thinner ones positioned opposite to each other to enable undistorted blood flow. The cross-section of the structure is not circular and becomes increasingly elongated as the cross-section moves towards the two thinner vessels, eventually taking on a shape similar to the digit 8 before splitting into two circular contours. Estimating the radius of a bifurcation using methods that assume a circular cross-sectional shape is difficult due to this non-circularity. Additionally, it is not possible to unambiguously determine the orientation of the vessel at the branching point, as the three vessels that meet there have different orientations.

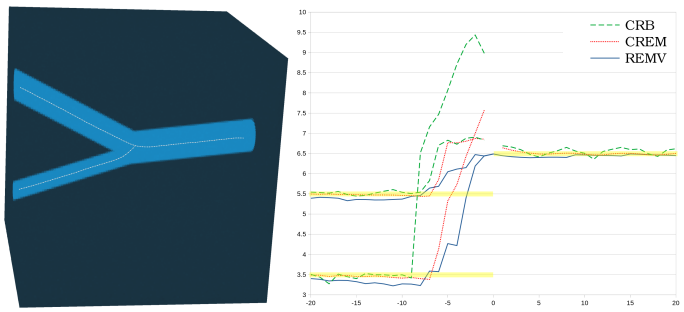

Fig. 5. The synthesized image of bifurcation and its estimated radii profiles.

The image of the bifurcation was synthesized with a background brightness of 64 and a structure brightness of 192, accounting for partial volume effects, and with additive Gaussian noise with a standard deviation of 1. Before applying

the radius estimation procedures, the image was binarized using a gray-level threshold of 128 and then skeletonized to extract centerlines [13,22,41]. The binary image was used for radius estimation by CRB, while the other methods estimated radii from the original gray-level image.

When comparing the results (Fig. 5), it can be observed that both CRB and CREM overestimate the radii of the thin blood vessels, and the estimated values near the bifurcation point exceed the radius of the thick vessel. In CRB, the estimated value is over three times higher than the actual one. Moreover, both methods exhibit a discontinuity in the radius estimation function at the branching point. The most accurate mapping of the radius near the bifurcation was obtained by REMV. Although the radii of thinner vessels are overestimated in the vicinity of the bifurcation point, the obtained values do not exceed the radii of the thicker vessel.

3.3 Radius estimation in MRA

No artificially generated model can capture all the properties and complexities of real angiograms. Therefore, it is necessary to verify if algorithms are capable of correctly estimating radii from genuine medical data. In the case of real images, no ground truth is available on the accurate values of blood vessels' radii. Therefore, the results presented in this section are visually inspected, and the evaluation is qualitative.

In this experiment, courtesy of Prof. Jürgen R. Reichenbach from University Hospital Jena, Germany, a 3D magnetic resonance angiogram (MRA) of a head is used (Fig. 6). The image was previously presented and used for validation of image processing algorithms in other publications [20,16]. It was acquired using the Time of Flight (ToF) Multiple Overlapping Thin Slab Acquisition (MOTSA) [28,2] procedure. The contrast between the flowing blood and the surrounding tissue is achieved without the use of a contrast agent, exclusively due to the dynamics of the flowing blood. In this technique, the stationary tissue is magnetically saturated and does not emit an electromagnetic echo. Fresh blood flowing into the saturated area, agitated by a radio frequency pulse, can emit this signal in contrast to the surrounding tissue. This imaging modality is minimally invasive and relatively comfortable and safe for patients. However, it may expose artifacts such as limited contrast if blood travels a long way in the saturation region, travels parallel to the slabs, or it may expose uneven brightness at the places where the slabs overlap. These artifacts make the image difficult to analyze.

The angiogram is characterized by relatively low spatial resolution. The voxel spacing is $0.42 \times 0.42 \times 1.2$ mm. This means that blood vessels less than 0.42 mm in diameter are poorly represented. Moreover, if vessels are located close to each other, at a distance of less than 0.42 mm, they may create false connections or merge into a single trace. The image shows vessels of various diameters, partly straight or curved, running close to each other or close to other structures. In addition, the occipital part of the image is brighter than the fronto-facial part. This data was deliberately selected as it is difficult to interpret and analyze,

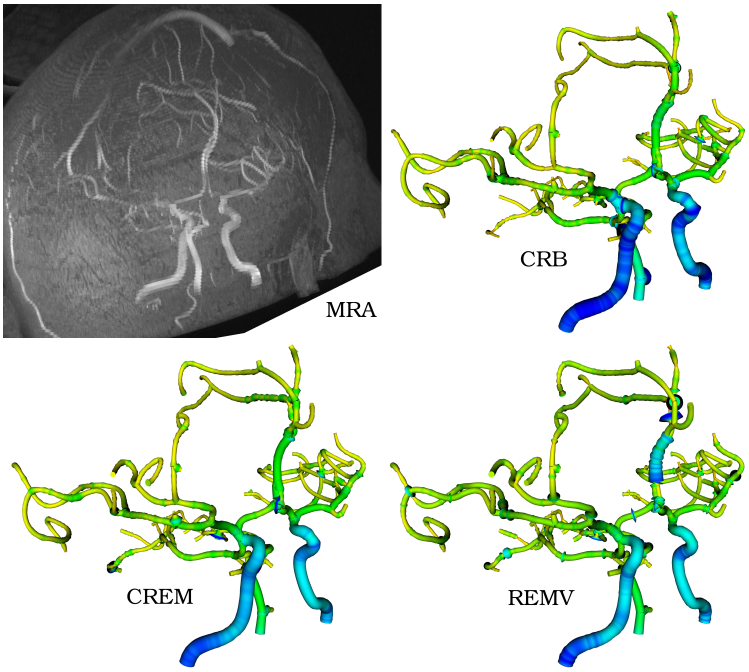

Fig. 6. The input MRA image and the resulting vessel system models.

which should enable the identification of shortcomings and potential limitations of the proposed algorithm.

The image was first enhanced and then binarized using a threshold value that was selected to extract blood vessels from other structures. A flood-fill algorithm was then applied to one of the main arteries to identify all vessels connected to it. The resulting volume was skeletonized to extract centerlines. In REMV, the vesselness function was computed for seven scales of σ ranging from 0.5 to 2.5. Fig. 6 displays the resulting models of blood vessel trees, which consist of tubes created around the centerlines. The tube radius varies locally based on the estimations generated by the algorithms under consideration.

There are two types of errors that can be visually identified. The first type of errors consists of moderate discrepancies scattered along the longer fragments of vessels. The second type consists of focal, yet distinct, radius overestimations, which appear as discs transversely oriented with respect to the course of the vessel. In the REMV model, most of the tube fragments appear smooth in comparison to the CRB or CREM models. Therefore, REMV does not have many visible errors of the first type. However, the number of second type of errors is the most pronounced in this method.

One of the unique structures of the blood vessel system in the brain are the two anterior cerebral arteries, which run close to each other. In the angiogram, the two arteries merge in the section where the distance between them is less

than the voxel size. The resulting single centerline is therefore incorrect since in reality there are two separate arteries. In CRB and CREM, the radius of the tube covering both arteries is small, and its surface is fairly smooth. In REMV, the radius is larger and uneven, which highlights the incorrectly extracted centerline.

4 Summary and conclusions

The paper presents an original REMV algorithm for estimating the radii of tubular structures in three-dimensional raster images, particularly medical angiographic images. The standard deviation of the Gaussian window at the maximum of the vesselness function, is a good estimator for vessel radius. A formula to approximate the function from a limited number of scales was found, making REMV computationally effective. Unlike CRB or CREM algorithms, which operate in the cross-sectional plane perpendicular to the vessel, REMV does not require prior information on the vessel's orientation. Moreover, the proposed method estimates the radius from the original grayscale image and does not require the image to be binarized, making it the method with the least requirements for initial input data.

Quantitative results from comparisons with reference methods show that REMV is the most accurate in estimating thin vessels. In comparison with CREM, another method that does not require image binarization, REMV seems to be immune to image noise and it is computationally more efficient. Furthermore, REMV yields the most accurate results in radius estimation in bifurcation, with radius overestimation being significantly smaller than in the other methods. Models derived from the real MRA were qualitatively assessed, and the REMV-based model is smooth; however, it exposes a few focal yet evident radius overestimations.

Table 2. Properties of the radius estimation algorithms.

	CRB	CREM	REMV
Input data requirements:			
Centerline orientation	Yes	Yes	No
Binary image	Yes	No	No
Estimation accuracy	Good	Fair	Good
Immunity to noise	N/A	Low	High
Computation speed	Fast	Slow	Moderate

Table 2 presents an overview comparison of the presented algorithms, taking into account three aspects: input data required by the method, accuracy of radius estimation for artificial images of cylinders, and computation time. It must be noted that immunity to noise of CRB depends on the preceding image segmentation method and is not an intrinsic property of this particular algorithm.

All the compared radius estimation algorithms were implemented in the Vesselknife program [36], which enables the visualization of three-dimensional raster images, their segmentation, extraction of blood vessel centerlines, estimation of radii, and visualization of the resulting models.

References

1. Antiga, L.: Generalizing vesselness with respect to dimensionality and shape. The Insight Journal **3**, 1–14 (2007)
2. Blatter, D.D., Parker, D.L., Robison, R.O.: Cerebral MR angiography with multiple overlapping thin slab acquisition. Part I. Quantitative analysis of vessel visibility. Radiology **179**(3), 805–811 (1991)
3. Blumenfeld, J., Kocinski, M., Materka, A.: A centerline-based algorithm for estimation of blood vessels radii from 3D raster images. In: 2015 Signal Processing: Algorithms, Architectures, Arrangements, and Applications (SPA). pp. 38–43 (Sep 2015)
4. Decroocq, M., Frindel, C., Ohta, M., Lavoué, G.: Modeling and hexahedral meshing of arterial networks from centerlines. arXiv:2201.08279 [cs] (Jan 2022)
5. Erdt, M., Raspe, M., Suehling, M.: Automatic hepatic vessel segmentation using graphics hardware. In: International workshop on medical imaging and virtual reality. pp. 403–412 (2008)
6. Feiniu Yuan, Yanling Chi, Su Huang, Jimin Liu: Modeling n-Furcated Liver vessels From a 3-D Segmented Volume Using Hole-Making and Subdivision Methods. IEEE Transactions on Biomedical Engineering **59**(2), 552–561 (Feb 2012)
7. Forkert, N.D., Säring, D., Fiehler, J., Illies, T., Möller, D., Handels, H.: Automatic Brain Segmentation in Time-of-Flight MRA Images. Methods of Information in Medicine **48**(05), 399–407 (2009)
8. Forkert, N.D., Schmidt-Richberg, A., Fiehler, J., Illies, T., Möller, D., Säring, D., Handels, H., Ehrhardt, J.: 3D cerebrovascular segmentation combining fuzzy vessel enhancement and level-sets with anisotropic energy weights. Magnetic Resonance Imaging **31**(2), 262–271 (Feb 2013)
9. Frangi, A.F., Niessen, W.J., Nederkoorn, P.J., Bakker, J., Mali, W.P., Viergever, M.A.: Quantitative analysis of vascular morphology from 3D MR angiograms: In vitro and in vivo results. Magnetic Resonance in Medicine **45**(2), 311–322 (Feb 2001)
10. Frangi, A.F., Niessen, W.J., Vincken, K.L., Viergever, M.A.: Multiscale vessel enhancement filtering. In: International conference on medical image computing and computer-assisted intervention. pp. 130–137 (1998)
11. Han, X., Bibb, R., Harris, R.: Design of bifurcation junctions in artificial vascular vessels additively manufactured for skin tissue engineering. Journal of Visual Languages & Computing **28**, 238–249 (Jun 2015)
12. Hilbert, A., Madai, V.I., Akay, E.M., Aydin, O.U., Behland, J., Sobesky, J., Galinovic, I., Khalil, A.A., Taha, A.A., Wuerfel, J.: BRAVE-NET: fully automated arterial brain vessel segmentation in patients with cerebrovascular disease. Frontiers in artificial intelligence p. 78 (2020)
13. Hong, Q., Li, Q., Wang, B., Tian, J., Xu, F., Liu, K., Cheng, X.: High-quality vascular modeling and modification with implicit extrusion surfaces for blood flow computations. Computer Methods and Programs in Biomedicine **196** (2020)

14. Izzo, R., Steinman, D., Manini, S., Antiga, L.: The Vascular Modeling Toolkit: A Python Library for the Analysis of Tubular Structures in Medical Images. Journal of Open Source Software **3**(25), 745 (May 2018)
15. Jerman, T., Pernuš, F., Likar, B., Špiclin, Ž.: Enhancement of vascular structures in 3d and 2d angiographic images. IEEE transactions on medical imaging **35**(9), 2107–2118 (2016)
16. Klepaczko, A., Szczypiński, P., Deistung, A., Reichenbach, J.R., Materka, A.: Simulation of MR angiography imaging for validation of cerebral arteries segmentation algorithms. Computer Methods and Programs in Biomedicine **137**, 293–309 (Dec 2016)
17. Klepaczko, A., Szczypiński, P., Dwojakowski, G., Strzelecki, M., Materka, A.: Computer Simulation of Magnetic Resonance Angiography Imaging: Model Description and Validation. PLOS ONE **9**(4) (2014)
18. Klepaczko, A., Szczypiński, P., Strzelecki, M., Stefańczyk, L.: Simulation of phase contrast angiography for renal arterial models. BioMedical Engineering OnLine **17**(1), 41 (Apr 2018)
19. Kociński, M., Klepaczko, A., Materka, A., Chekenya, M., Lundervold, A.: 3d image texture analysis of simulated and real-world vascular trees. Computer methods and programs in biomedicine **107**(2), 140–154 (2012)
20. Kociński, M., Materka, A., Deistung, A., Reichenbach, J.R.: Centerline-based surface modeling of blood-vessel trees in cerebral 3D MRA. In: 2016 Signal Processing: Algorithms, Architectures, Arrangements, and Applications (SPA). pp. 85–90 (2016)
21. Lamy, J., Merveille, O., Kerautret, B., Passat, N., Vacavant, A.: Vesselness filters: A survey with benchmarks applied to liver imaging. In: 2020 25th International Conference on Pattern Recognition (ICPR). pp. 3528–3535 (2021)
22. Lee, T.C., Kashyap, R.L., Chu, C.N.: Building skeleton models via 3-D medial surface axis thinning algorithms. CVGIP: Graphical Models and Image Processing **56**(6), 462–478 (1994)
23. Lesage, D., Angelini, E.D., Bloch, I., Funka-Lea, G.: A review of 3D vessel lumen segmentation techniques: Models, features and extraction schemes. Medical Image Analysis **13**(6), 819–845 (Dec 2009)
24. Litjens, G., Ciompi, F., Wolterink, J.M., de Vos, B.D., Leiner, T., Teuwen, J., Išgum, I.: State-of-the-Art Deep Learning in Cardiovascular Image Analysis. JACC: Cardiovascular Imaging **12**(8), 1549–1565 (Aug 2019)
25. Livne, M., Rieger, J., Aydin, O.U., Taha, A.A., Akay, E.M., Kossen, T., Sobesky, J., Kelleher, J.D., Hildebrand, K., Frey, D., Madai, V.I.: A U-Net Deep Learning Framework for High Performance Vessel Segmentation in Patients With Cerebrovascular Disease. Frontiers in Neuroscience **13** (2019)
26. Lorensen, W.E., Cline, H.E.: Marching cubes: A high resolution 3D surface construction algorithm. ACM siggraph computer graphics **21**(4), 163–169 (1987)
27. Materka, A., Kociński, M., Blumenfeld, J., Klepaczko, A., Deistung, A., Serres, B., Reichenbach, J.R.: Automated modeling of tubular blood vessels in 3D MR angiography images. In: 2015 9th International Symposium on Image and Signal Processing and Analysis (ISPA). pp. 54–59 (2015)
28. Parker, D.L., Yuan, C., Blatter, D.D.: MR angiography by multiple thin slab 3D acquisition. Magnetic resonance in medicine **17**(2), 434–451 (1991)
29. Piccinelli, M., Veneziani, A., Steinman, D., Remuzzi, A., Antiga, L.: A Framework for Geometric Analysis of Vascular Structures: Application to Cerebral Aneurysms. IEEE Transactions on Medical Imaging **28**(8), 1141–1155 (Aug 2009)

30. Quarteroni, A., Manzoni, A., Vergara, C.: The cardiovascular system: Mathematical modelling, numerical algorithms and clinical applications *. Acta Numerica **26**, 365–590 (May 2017)
31. Ronneberger, O., Fischer, P., Brox, T.: U-net: Convolutional networks for biomedical image segmentation. In: International Conference on Medical image computing and computer-assisted intervention. pp. 234–241 (2015)
32. Rudyanto, R.D., Kerkstra, S., Van Rikxoort, E.M., Fetita, C., Brillet, P.Y., Lefevre, C., Xue, W., Zhu, X., Liang, J., Öksüz, I., et al.: Comparing algorithms for automated vessel segmentation in computed tomography scans of the lung: the vessel12 study. Medical image analysis **18**(7), 1217–1232 (2014)
33. Sato, Y., Nakajima, S., Atsumi, H., Koller, T., Gerig, G., Yoshida, S., Kikinis, R.: 3D multi-scale line filter for segmentation and visualization of curvilinear structures in medical images. In: Troccaz, J., Grimson, E., Mösges, R. (eds.) CVRMed-MRCAS'97. pp. 213–222. Berlin, Heidelberg (1997)
34. da Silva, M.V., Ouellette, J., Lacoste, B., Comin, C.H.: An Analysis of the Influence of Transfer Learning When Measuring the Tortuosity of Blood Vessels. arXiv:2111.10255 [cs, eess] (Jan 2022)
35. Smistad, E., Falch, T.L., Bozorgi, M., Elster, A.C., Lindseth, F.: Medical image segmentation on GPUs – A comprehensive review. Medical Image Analysis **20**(1), 1–18 (Feb 2015)
36. Szczypinski, P.M.: Vesselknife, `https://gitlab.com/vesselknife/vesselknife`
37. Vinhais, C., Kociński, M., Materka, A.: Centerline-Radius Polygonal-Mesh Modeling of Bifurcated Blood Vessels in 3D Images using Conformal Mapping. In: 2018 Signal Processing: Algorithms, Architectures, Arrangements, and Applications (SPA). pp. 180–185 (Sep 2018)
38. Wink, O., Niessen, W., Viergever, M.: Fast delineation and visualization of vessels in 3-D angiographic images. IEEE Transactions on Medical Imaging **19**(4), 337–346 (Apr 2000)
39. Woźniak, T., Strzelecki, M., Majos, A., Stefańczyk, L.: 3D vascular tree segmentation using a multiscale vesselness function and a level set approach. Biocybernetics and Biomedical Engineering **37**(1), 66–77 (2017)
40. Yang, G., Kitslaar, P., Frenay, M., Broersen, A., Boogers, M.J., Bax, J.J., Reiber, J.H.C., Dijkstra, J.: Automatic centerline extraction of coronary arteries in coronary computed tomographic angiography. The International Journal of Cardiovascular Imaging **28**(4), 921–933 (Apr 2012)
41. Zasiński, P., Kociński, M., Materka, A.: On extracting skeletons from binary 3D images. In: 2017 International Conference on Systems, Signals and Image Processing (IWSSIP). pp. 1–5 (May 2017)
42. Zeng, Y.z., Liao, S.h., Tang, P., Zhao, Y.q., Liao, M., Chen, Y., Liang, Y.x.: Automatic liver vessel segmentation using 3D region growing and hybrid active contour model. Computers in Biology and Medicine **97**, 63–73 (Jun 2018)
43. Zhao, J., Zhao, J., Pang, S., Feng, Q.: Segmentation of the True Lumen of Aorta Dissection via Morphology-constrained Stepwise Deep Mesh Regression. IEEE Transactions on Medical Imaging pp. 1–1 (2022)
44. Zhao, Y., Rada, L., Chen, K., Harding, S.P., Zheng, Y.: Automated Vessel Segmentation Using Infinite Perimeter Active Contour Model with Hybrid Region Information with Application to Retinal Images. IEEE Transactions on Medical Imaging **34**(9), 1797–1807 (Sep 2015)